A NEW METHOD OF DATA ASSIMILATION BASED ON ENSEMBLE KALMAN FILTER WITH APPLICATION TO COASTAL ACOUSTIC TOMOGRAPHY DATA

Minmo Chen[1], Arata Kaneko[1], Ju Lin[2], Chuanzheng Zhang[3]

[1] Graduate School of Engineering, Hiroshima University, 1-4-1 Kagamiyama, Higashi-Hiroshima 739-8527, JAPAN
[2] College of Information Science & Engineering, Ocean University of China, Qingtao, CHINA
[3] State Key Laboratory of Satellite Ocean Environment Dynamics, Second Institute of Oceanography, State Oceanic Administration, Hangzhou, CHINA

Minmo Chen, Graduate School of Engineering, Hiroshima University, 1-4-1 Kagamiyama, Higashi-Hiroshima 739-8527, JAPAN. Fax: (+81) 82 424 7863, e-mail: d153155@hiroshima-u.ac.jp

Abstract: *A new method of data assimilation (DA) based on ensemble Kalman filter with less time-consuming properties is proposed here. In this method, model error covariance is determined from the perturbed model state vectors at each DA time without forecasting the ensemble model state vectors. A smooth correlation function is introduced to model error covariance to localize the tomography domain. The model state vectors are perturbed by a N-ensemble of smooth pseudorandom fields, the sub-vectors of which have zero mean and adjustable variance. Furthermore, their covariance is determined from the decorrelation length. Thus, the proposed method is different from the conventional method in which model error covariance is calculated through an ensemble procedure of the model at every time growth. The method was successfully applied to assimilate the 2013 Hiroshima Bay coastal acoustic tomography (CAT) data into a baroclinic ocean model based on POM (Princeton Ocean Model). A coastal upwelling, generated along the northern shore of Hiroshima Bay by a northerly wind from a typhoon, was well structured in a two-layer system of current and salinity. The data assimilation results were validated with path-average CAT and CTD data*

and the estimated errors were smaller than variation ranges of current and salinity, associated with the upwelling.

Keywords: *CAT, data assimilation, ensemble Kalman filter, coastal upwelling, Hiroshima Bay*

1. INTRODUCTION

Coastal acoustic tomography (CAT), an application of ocean acoustic tomography to coastal seas, constructs the spatial structures of ~~a~~ current and ~~of~~ sound speed (temperature and/or salinity), the accuracy of which has been validated in comparison to ADCP and CTD data [1]-[7]. Data assimilation (DA) has been developed as an innovative method to improve the model simulated field significantly by the ocean acoustic tomography data. Noticeable efforts assimilating CAT data into the barotropic ocean model with ensemble Kalman filter (EnKF) have been executed by Park and Kaneko [8] and Ju Lin et al. [9].

The conventional EnKF methods are derived from merging Kalman filter theory and Monte Carlo estimate [10]-[11]. In these methods, the model error covariance is estimated from ensemble forecasts growing with a time step. For typical oceanic applications, the process for constructing the ensemble forecasts and the model error covariance is a major source to increase the computational time exhausted for completing a DA cycle. The large ensemble size is needed to attain the accurate model error covariance so that much computational time is consumed.

A new method of data assimilation with much time reduction based on EnKF is proposed here in which the model error covariance is calculated from pseudorandom fields provided in a fixed time without time growths. Application results of this method to the 2013 Hiroshima Bay coastal acoustic tomography data are reported.

2. OBSERVATION DATA

A CAT experiment with four acoustic stations (H1, H2, H3 and H5) was conducted from September 11 to 25, 2013 in Hiroshima Bay (Fig. 1). The conductivity-temperature-depth (CTD) data were acquired at 10 stations (C1-C10) on the sound transmission lines on September 18. The CTD data were used to construct sound speed fields that were then used for acoustic ray trace predictions in the tomography domain with the vertical profile of temperature from September 17, provided by the Hiroshima City Fisheries Promotion Centre (HCFPC). Long-term temperature profiles were obtained at depths of 0, 2, 4, 7, 10 and 15 m every 5 minutes from August 1 to October 23 using a temperature array, placed at T1. They served the sound speed-to-salinity conversion using the sound speed formula and the resulting salinity assimilation. The data assimilation results of salinity were validated with the CTD data.

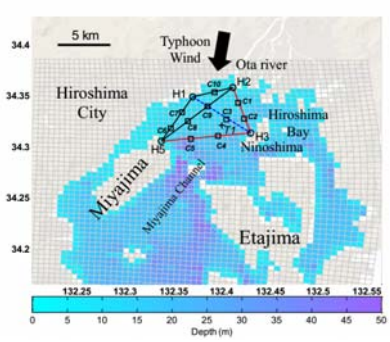

Fig. 1: The CAT experiment domain. The four CAT acoustic stations (H1, H2, H3 and H5) and ten CTD cast points (C1-C10) are indicated with circles and squares, respectively. The black lines connecting the acoustic stations show the reciprocal sound transmission lines and the red lines the one-way sound transmission lines. The blue dashed line is the transmission line with no data. T1 is the temperature array position. A distance scale of 5 km is at the top-left corner of the panel. A color scale for depth is at the bottom of the figure.

Two reciprocal arrival peaks were successfully identified among H1, H2 and H5, constructing a triangular array (Fig. 1). However, only one-way data of first peaks could be identified for H2H3 and H3H5 owing to the H3 system having a poor performance. Correlation patterns for the received signals are shown in upper panel of Fig 2 with the stack diagrams and the ray simulation result in the lower panel. The green and red dots correspond to arrival peaks for the surface-bottom reflected (SBR) rays and surface reflected (SR) rays, respectively. The SBR rays with reflection numbers smaller than the SR rays were the first arrivals and largest peaks for H2H5 and H5H1 while the SR rays with reflection numbers smaller than the SBR rays were the first arrivals and largest peaks for H1H2. The SR rays were the second arrival for H2H5 and H5H1 while the SBR rays were the second arrival for H1H2. The SBR rays that passed through the whole depth from the surface to the bottom sampled the depth-average current and sound speed. Hence, information from the SBR rays is suitable to be assimilated into the model results as the barotropic (depth-average) data, thus being called a barotropic data assimilation (BTDA). On the other hand, the SR rays passed only through the upper 5 m and give baroclinic information to the model, thus called a baroclinic data assimilation (BCDA).

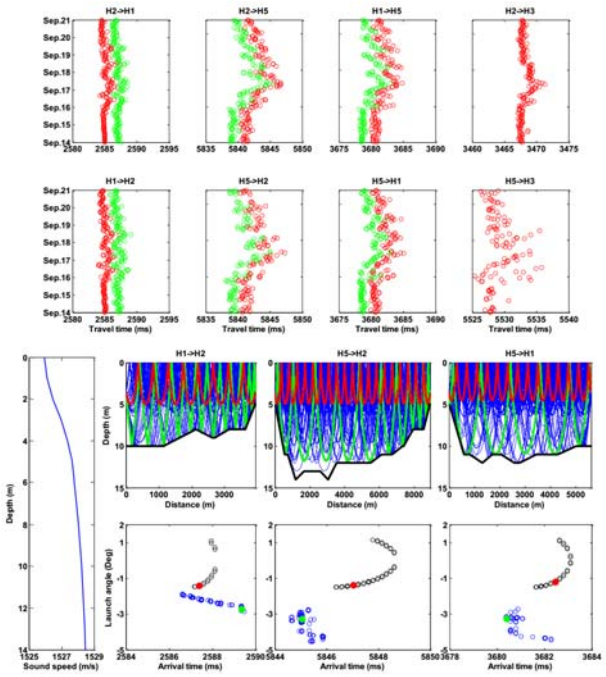

Fig. 2: Upper panel: Stack diagrams of the received correlation patterns plotted with the time axis proceeding upward. Lower panel: Results of range-independent ray simulation along the three reciprocal transmission lines H1H2, H2H5 and H5H1. The green and red lines show the SBR and SR rays, respectively. Green and red dots indicate arrival peaks for the SBR and SR rays, respectively.

3. METHOD

In the proposed method, to account for model error covariance P in a DA cycle, N-ensemble pseudorandom fields are directly added to the forecast result. N is taken 250 in this study. Each sub-vector of the pseudorandom fields has a zero mean and time invariant variance equal to certain value. The covariance among each sub-vector is determined by the decorrelation length given to fit the observation domain prior to the covariance calculation. Covariance localization is implemented using a product of the ensemble-based covariance with a smooth correlation function to localize the effect of data assimilation inside the tomography domain [12]. The smooth correlation function used here is defined by Gaspari and Cohn [13], using a 5^{th} order piecewise polynomial function which decrease to 0 at a certain distance from the center of tomography domain. The observation error covariance R is determined from the variation of CAT travel times, typically using standard deviation (STD) in a short-period range of 10 min to one hour.

Another specific aspect of this method is that the model error covariance is an adjustable variable relative to the observation error. The optimal value of ratio P/R was thought from the root mean square errors (RMSEs) for the DA path-average currents and CAT path-average current plotted against the ratio of P/R. The ratio was determined 12 at the point where the decreasing rate of RMSD was largely reduced.

In the DA cycle, the difference of travel-time perturbations for the first arrival peak at H2H5 and H5H1, and for the second arrival peak at H1H2, corresponding to the SBR rays, was firstly assimilated into the barotropic component of the current (barotropic assimilation). The sum of

travel time perturbations for the SBR rays at H1H2, H2H5 and H5H1 and the one-way travel time of travel-time perturbations for the SBR rays at H2H3 and H3H5 were also assimilated in the barotropic component of salinity (barotropic assimilation). The barotropic DA results served to adjust the baroclinic model result. The difference of travel-time perturbations for the second arrival peak at H2H5 and H5H1, and for the first arrival peak at H1H2 were related to the SR rays. The SR rays only passed through the upper 5 m and provided baroclinic information for the model. This baroclinic information was assimilated into the baroclinic model with ten vertical grids (baroclinic assimilation). Furthermore, the sum of travel-time perturbations for the SR rays at H1H2, H2H5 and H5H1 were incorporated into the salinity in the 9-layer baroclinic model (baroclinic assimilation).

Only two arrival peaks or two rays were resolvable in the observation data because the profiles of sound speed and salinity were characterized by the upper and lower layers separated by a steep slope at the 5-m depth (see the lower panel of Fig 2). The result of the 9-layer data assimilation was therefore well approximated by the 2-layer result, averaging the upper and lower layers.

4. RESULTS

The DA results are shown in Fig 3 with the 6-hour interval vector plots for the subtidal component (mainly the wind-driven current), averaged over the upper and lower layers. The subtidal current was less than 0.02 ms^{-1} before the maximum northerly wind blew over the bay at 10:00 of September 16 and strengthened with the decrease of the northerly wind after it reached the maximum. Around the northern part of the bay during 00:00-12:00 of September 17 the subtidal currents were directed southward in the upper layer while the lower layer was directed by the northward current. During this mature phase of the upwelling, the magnitude of the subtidal current reached 0.10 ms^{-1} for the upper layer and 0.08 ms^{-1} for the lower layer. As time proceeded, the southward upper-layer current gradually diminished and was replaced by the northeastward current with a maximum value of 0.10 ms^{-1} from the beginning of September 19. During this period, the lower-layer current with magnitudes lower than 0.05 ms^{-1} also shifted from the north to the southeast especially in the eastern half of the bay.

The DA salinity results for the 2-day filtered data are shown in Fig 4 with the contour plots for the upper- and lower-layer averages. With the start of salinity assimilation at 00:00 on September 15, a salinity contrast of 28.5 and 29.5 developed between the upper and lower layers except for the northern shore region which displayed unnaturally high salinity of 32. This contrast continued up to 06:00 of September 16. In the upper layer, a tongue of saline water greater than S=31 begun to develop southward from the northern shore of the bay at 18:00 on September 16 and reached a mature phase during 00:00-12:00 of September 17. Outside the tongue, the upper-layer salinity was 30.0-30.5 lesser than the lower-layer salinity of 30.5-31.0. After the mature phase, the upper-layer saline tongue gradually retreated northeastward with a reduced speed up to the end of September 19. From September 18 to 19, the upper-layer salinity gradually decreased from 30.5 to 30.0 except for in the tongue region. At the same time, the lower-layer salinity stayed almost constant in the range of 30.5-31.0.

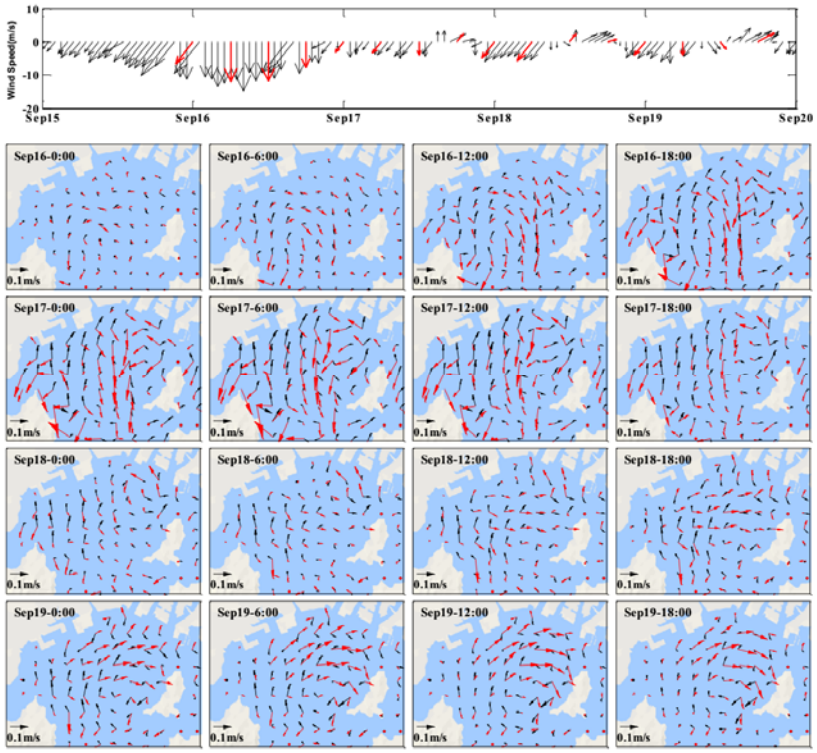

Fig. 3: The 6-hour interval variations of the subtidal BCDA currents for the upper-layer (red arrows) and lower-layer (black arrows) from 00:00 of September 16 to 18:00 of September 19. The temporal variation of wind vectors is also shown at the top of the figure. The thick red arrows on the wind speed plot are placed at the times corresponding to the 6-hour interval current pictures. A scale of 0.1 ms^{-1} is provided at the bottom-left corner of each figure.

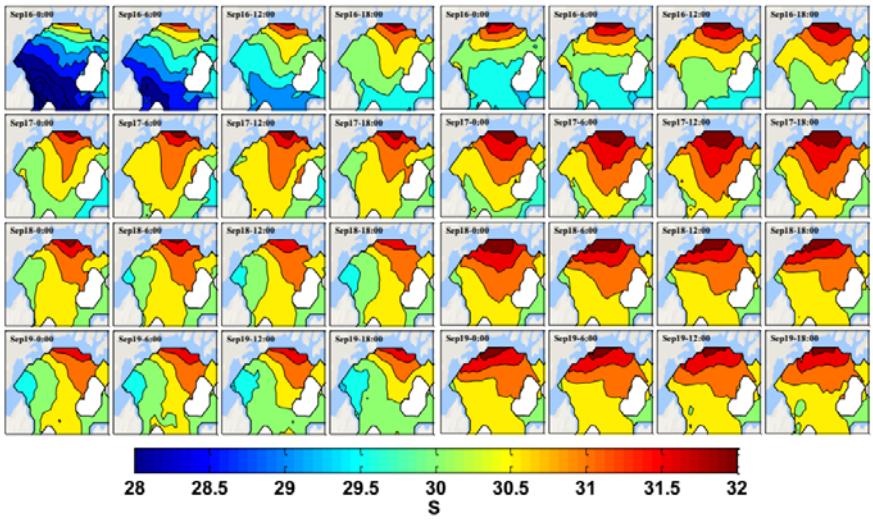

Fig. 4: The 6-hour interval variations of the 2-day filtered DA salinity, averaged for the upper (left) and lower (right) layers. A color bar for salinity is provided at bottom of the figure.

The 10-grid profiles of the 2-day filtered BCDA salinity are compared with the CTD data in Fig 5. The BCDA salinity profiles overestimated the CTD salinities at C1 and C10 close to

the northern shore and underestimated the CTD salinities at C5, C6, C7 and C8 southwest of the tomography domain. The assimilation of the fixed-point temperature array data for the whole domain produced misfits with the salinity at the CTD points located far from the temperature array. Note that the water was well homogenized from the surface to the bottom in the POM results.

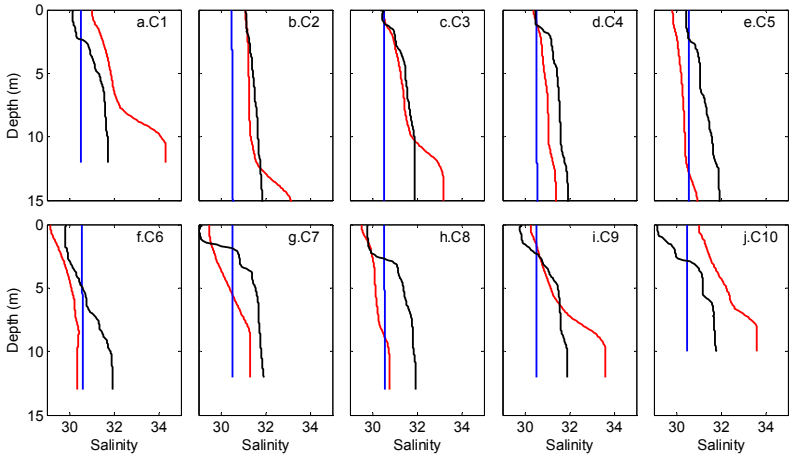

Fig. 5: The 10-grid profiles of the 2-day filtered BCDA (red line) and POM (blue line) salinities in comparison with the 10-point CTD data (black line).

5. SUMMARY

The proposed method of data assimilation was applied to assimilate the CAT data into the baroclinic ocean model based on POM (Princeton Ocean Model). The 3D process of coastal upwelling and the associated reverse flow, generated in the northern part of Hiroshima Bay, was well reconstructed by the assimilation of the barotropic and the baroclinic data from CAT. As proposed by Munk et al. [14], it is confirmed that the CAT data is the precious partner of data assimilation best fitted to the ocean model.

REFERENCE

[1] H. Zheng, N. Gohda, H. Noguchi, T. Ito, H. Yamaoka, T. Tamura, Y. Takasugi and A. Kaneko, Reciprocal sound transmission experiment for current measurement in the Seto Inland Sea, Japan, *J. Oceanogr.*, vol. 53, pp. 117-127, 1997.

[2] J.-H. Park and A. Kaneko, Assimilation of coastal acoustic tomography data into a barotropic ocean model, *Geophys. Res. Lett.*, vol. 27, pp. 3373-3376, 2000.

[3] H. Yamaoka, A. Kaneko, J.-H. Park, H. Zheng, N. Gohda, T. Takano, X.-H. Zhu and Y. Takasugi, Coastal acoustic tomography system and its field application, *IEEE J. Oceanic Eng.*, vol. 27, pp. 283-295, 2002.

[4] K. Yamaguchi, J. Lin, A. Kaneko, T. Yamamoto, N. Gohda, H.-Q. Nguyen and H. Zheng, A continuous mapping of tidal current structures in the Kanmon Strait, *J. Oceanogr.*, vol. 61, pp. 283-294, 2005.

[5] X.-H. Zhu, A. Kaneko, Q.-S. Wu, C.-Z. Zhang, N. Taniguchi and N. Gohda, Mapping Tidal Current Structures in Zhitouyang Bay, China, using Coastal Acoustic Tomography, *IEEE J. Oceanic Eng.*, vol. 38, pp. 285-296, doi: 10.1109/JOE.2012.2223911, 2013.

[6] X.-H. Zhu, Z.-N. Zhu, X. Guo, Y.-L. Ma, X. Fan, M.-H. Dong and C.-Z. Zheng,

Measurement of tidal and residual currents and volume transport through the Qiongzhou Strait using coastal acoustic tomography, *Continental Shelf Res*., vol. 108, pp. 65-75, 2015.

[7] C.-Z. Zhang, A. Kaneko, X.-H. Zhu and N. Gohda, Tomographic mapping of a coastal upwelling and the associated diurnal internal tides in Hiroshima Bay, Japan, *J. Geophys. Res.*, doi:10.1002/2014JC010676, pp. 4288-4305, 2015.

[8] J.-H. Park and A. Kaneko, Assimilation of coastal acoustic tomography data into a barotropic ocean model, *Geophys. Res. Lett.*, vol. 27, pp. 3373-3376, doi:10.1029/ 2000GL011600, 2000.

[9] J. Lin, A. Kaneko, N. Gohda and K. Yamaguchi, Accurate imaging and prediction of Kanmon Strait tidal current structures by the coastal acoustic tomography data, *Geophys. Res. Lett.*, 32, L14607, doi:10.1029/ 2005GL022914, 2005.

[10] G. Evensen, Sequential data assimilation with a nonlinear quasi□geostrophic model using Monte Carlo methods to forecast error statistics, *J. Geophys. Res.*, vol. 99, pp. 10143-10162, 1994.

[11] G. Evensen, The ensemble Kalman filter: Theoretical formulation and practical implementation, *Ocean dynamics*, vol. 53, pp. 343-367, 2003.

[12] P. L. Houtekamer and H. L. Mitchell, A sequential ensemble Kalman filter for atmospheric data assimilation, *Mon. Weather Rev.*, vol. 129, pp. 123-137, 2001.

[13] G. Gaspari and S. E. Cohn, Construction of correlation functions in two and three dimensions, *Quart. J. Roy. Meteor. Soc.*, vvol.125, pp. 723–757, 1999.

[14] W. Munk, P. F. Worcester and C. Wunsch, *Ocean Acoustic Tomography*, New York: Cambridge Univ. Press, 433pp, 1995.